Applied Catalysis B: Environmental 87 (2009) 9–17

Contents lists available at ScienceDirect

Applied Catalysis B: Environmental

journal homepage: www.elsevier.com/locate/apcatb

Ageing and SO_2 resistance of Pd containing perovskite-type oxides

E. Tzimpilis [a,*], N. Moschoudis [a], M. Stoukides [a,b], P. Bekiaroglou [a]

[a] Department of Chemical Engineering, Aristotle University of Thessaloniki, 54124 Thessaloniki, Greece
[b] Chemical Process Engineering Research Institute, University Box 1517, 54124 Thessaloniki, Greece

ARTICLE INFO

Article history:
Received 9 June 2008
Received in revised form 22 August 2008
Accepted 26 August 2008
Available online 31 August 2008

Keywords:
Pd catalysts
Pd–perovskites
Natural gas vehicles
Ageing
SO_2 poisoning

ABSTRACT

The $La_{0.91}Mn_{0.85}Ce_{0.24}Pd_{0.05}O_z$ and $La_{1.034}Mn_{0.966}Pd_{0.05}O_z$ perovskite-type oxides were prepared via a combination of the sol–gel and the combustion synthesis methods. They were characterized by X-ray diffraction, X-ray photoelectron spectroscopy, energy dispersive X-ray, high resolution transmission electron microscopy and electron energy loss spectroscopy. The effect of ageing and SO_2 on the catalytic effectiveness of the Pd/perovskite and of a Pd-based commercial three-way catalyst for stoichiometrically operating natural gas fuelled vehicles were investigated. The $La_{1.034}Mn_{0.966}Pd_{0.05}O_z$ catalyst exhibited the highest thermal stability and, in contrast to the $La_{0.91}Mn_{0.85}Ce_{0.24}Pd_{0.05}O_z$ and the commercial catalyst, it appeared significantly activated in the presence of 8 ppm SO_2 in the reactant mixture. The formation of La–Pd mixed oxides or/and $La_2(Mn–Pd)O_6$, the enhanced surface Pd^{2+} composition and the low surface sulfur content were suggested as the possible reasons for the activation under sulfur environment.

1. Introduction

The catalytic exhaust aftertreatment of stoichiometrically operating natural gas fuelled vehicles (NGFVs) is necessary for the abatement of methane, carbon monoxide and nitrogen oxides. The catalytic combustion of methane has been widely investigated in the last decades. Oxidized Pd, supported on various metal oxides, mainly Al_2O_3 and SiO_2, was found as the most active catalyst. Also, perovskite-type oxides have received remarkable attention since the 1970s as catalysts for the complete oxidation of hydrocarbons (HCs) because of their low cost and high thermal stability [1,2]. They are represented by the general formula ABO_3, where A is a rare earth metal cation and B is a transition metal cation.

The structural and physico-chemical characteristics of perovskite-type oxides, as well as their catalytic properties for various reactions, depend on the phase composition and on the preparation method and its parameters [3–7]. The effectiveness of both of the above catalytic systems is strongly influenced by the composition of the reaction mixture. Water, CO_2 and sulfur compounds have a negative effect on catalytic activity [8–12].

Palladium/metal oxide materials, used for the catalytic oxidation of HCs, especially of methane, are known to exhibit severe deactivation when sulfur compounds are present in the feed stream [13–15]. Under 10 ppm SO_2 containing reactant mixture, a remarkable loss of the activity was observed in a PdO/alumina catalyst for the lean-burn NGFVs application. This catalytic activity loss was attributed to the increased rate of bulk $PdSO_4$ formation, caused by spillover of sorbed SO_2 and SO_3 species from the alumina support to the PdO surface [16]. The spillover was favored by the presence of water, a product of methane combustion. Exposure of Pd/Al_2O_3 and Pt/Al_2O_3 to H_2S, for the same application, implied a severe and irreversible deactivation for the former, while the latter appeared more resistant. The formation of inactive $PdSO_4$ was suggested as the reason for the Pd/Al_2O_3 deactivation [11]. A similar behavior was observed with Pd/Al_2O_3 and Rh/Al_2O_3 catalysts in the presence of either SO_2 or H_2S [17]. The presence of either sulfur species increased the catalytic activity of Pt/Al_2O_3 because of an increase in acidity, which in turn, was caused by the formation of aluminum sulfates on the support. SO_2 was also found to have a positive effect on the activity of Pt during propane oxidation. Various explanations were suggested, such as enhanced propane chemisorption on oxidized Pt [18], or, polarization by sulfation of atoms at perimeter sites at the platinum/support interface [19]. In a previous study [20], it was reported that, although the PdO/ZrO_2 catalyst exhibited deactivation upon introduction of 20 ppm SO_2 in the feed stream, a dramatic enhancement in effectiveness was observed when the catalyst was pretreated at 400 °C for 1 h in a mixture containing 20 ppm SO_2. The acidity of the SO_2 pretreated PdO/ZrO_2 catalyst was

* Corresponding author. Tel.: +30 2310996178; fax: +30 2310996222.
E-mail address: tzimpi@auth.gr (E. Tzimpilis).

0926-3373/$ – see front matter © 2008 Elsevier B.V. All rights reserved.
doi:10.1016/j.apcatb.2008.08.020

increased and its activation was related to the formation of a composite site between the PdO and the acidic sulfate at the PdO/ZrO_2 interface.

The presence of sulfur compounds has a negative effect on the activity of perovskite-type oxides for methane combustion [21]. The $LaMn_{1-x}Mg_xO_3$ catalysts were found to drastically deactivate by the introduction of 200 ppm SO_2 at 800 °C for 24 h [22]. In particular, $LaMn_{0.5}Mg_{0.5}O_3$ was deactivated by the formation of surface magnesium sulfate, while $LaMn_{0.8}Mg_{0.2}O_3$ and $LaMnO_3$ were poisoned by lanthanum sulfate formation. The SO_2 resistance of $LaMn_{1-x}Mg_xO_3{\cdot}yMgO$ increased substantially when MgO was used as an additive [23]. The increase of the MgO content increased the protection from SO_2, which was attributed to the formation of sulfate species on the MgO phase. Replacement of Mn by Cr in the $LaMn_{1-x}Mg_xO_3$ catalysts induced lower catalytic activity in the fresh state, but decreased the adsorption of SO_2 on the perovskite, resulting in higher resistance to sulfur poisoning [24]. The activity loss of the $La_{0.8}Ce_{0.2}MnO_3$ after exposure to SO_2, either by dielectric or by conventional heating, was attributed to the formation of lanthanum sulfate [25]. In the case of conventional heating, deactivation was faster because of the pore blockage at the outer core. The deactivation of $La_{1-x}Ce_xMn_{1-y}Co_yO_3$ by SO_2 was ascribed to the formation of $La_2(SO_4)_3$, while prolonged exposure to SO_2 or H_2S led to the partial catalyst decomposition with the formation of $La_2(SO_4)_3$, CeO_2 and Co_3O_4 [26]. Decomposition by sulfur compounds was also reported for the $LaCoO_3$ perovskite [27].

Addition to or incorporation in the perovskite structure of small amounts of noble metals, was reported to enhance their catalytic activity as well as their sulfur resistance [21,28,29]. In a recent study, an increase in the Pd content of $Pd/LaMn_{1-x}Fe_xO_3$ catalysts, was found to favor sulfur resistance. It was suggested that sulfur attack begins by reacting with the Pd particles; after all Pd is covered, lanthanum sulfates are formed [30].

Currently used commercial Pd-based three-way catalysts (TWC) for stoichiometrically operating NGFVs, contain high quantities of noble metals. In a previous study [31], efforts to reduce the Pd content resulted in the $La_{0.91}Mn_{0.85}Ce_{0.24}Pd_{0.05}O_z$ and $La_{1.034}Mn_{0.966}Pd_{0.05}O_z$ perovskites, which exhibited promising results in terms of the above application. The present work focuses on the effects of prolonged hydrothermal ageing and SO_2 poisoning on the catalytic performance of these active phases, under simulated exhaust conditions. Results are compared to a currently used Pd-based commercial catalyst, containing an almost threefold higher noble metal load.

2. Experimental

2.1. Catalysts preparation

The $La_{0.91}Mn_{0.85}Ce_{0.24}Pd_{0.05}O_z$ and $La_{1.034}Mn_{0.966}Pd_{0.05}O_z$ active phases were prepared via a combination of the sol–gel and the combustion synthesis methods. Amounts corresponding to the stoichiometry of the formulation of 2 M aqueous solutions of the metal nitrates, were used for the preparation of the precursor solution. Excess glycine was added in order to achieve complexation of the metal ions. Water was removed from the produced homogenous precursor solutions by evaporation at 115 °C for 24 h. An amorphous material was obtained, which was crushed and calcined in air, at 750 °C, for 1 h. Further details on the preparation procedure can be found in a previous communication [31].

The obtained catalytic powders were tested in the monolithic form in order to approach real conditions and to be able to compare to a commercial catalyst. The powders were deposited on monolithic cordierite substrates of 400 cpsi (6 × 6 cells, 18 mm length) by immersion in slurries prepared by mixing active phase powders and *n*-butanol, followed by drying at 120 °C and calcination in air at 750 °C for 1 h. The Pd load of the resulted Pd/perovskite catalysts was approximately 120 g ft^{-3} (1 g Pd ft^{-3} = 0.035315 kg Pd m^{-3}). The same sized trimetallic (Pt/Pd/Rh) currently used commercial catalyst contained 300 g of noble metals per ft^{-3}.

2.2. Catalytic activity measurements

A quartz tubular reactor was used for the catalytic activity tests and for the high temperature hydrothermal treatments. The inlet temperature was measured by a thermocouple placed at the front side of the monolith. The temperature programmed reaction technique in the range 300–800 °C was applied for the tests. The samples were warmed up at a rate of 10 °C min^{-1} and were freely cooled down. The catalysts were cooled down from 800 to 300 °C prior to the tests in order to be activated as described previously [31].

The gas feed redox characteristics were adjusted by the stoichiometric number R_x, which is defined as the ratio of the sum of the equivalents of oxidants (oxygen, nitrogen monoxide) to the sum of the equivalents of reductants (methane, carbon monoxide). Ageing of the monoliths was carried out in the reactor at 950 °C for several hours, using the reactant mixture with composition no. 1 of Table 1. The catalysts were tested in the fresh state and after 3, 6 and 12 h of ageing. Simulation of representative exhaust conditions for the stoichiometrically operating NGFVs was achieved by the use of a reactant mixture with composition no. 2 of Table 1. The SO_2 effect was investigated on catalysts aged for 3 h at 950 °C. Continuous operation under SO_2 environment affected, positively or negatively, the catalysts during the first 20 h. Longer exposures had essentially no effect on the catalytic activity and, therefore, the final activity was evaluated after 22 h in the SO_2 environment. Measurements were taken after 3, 5, 7.5, 12.5 and 22 h of exposure and under SO_2-free environment.

The presence of more than one reductants (CO – CH_4), more than one oxidants (O_2 – NO), as well as the presence of H_2O and CO_2 (the latter are known to cause deactivation), make the reaction system much more complicated than when only one oxidant reacts with one reductant. Therefore, calculation of rates (or normalized rates) and of activation energies, will not contribute substantially in the elucidation of the mechanism of the involved reactions. Thus, the catalytic results are presented in plots of conversion vs. temperature.

A series of continuous analyzers, FID PM-1 (Pierburg) for total hydrocarbons, NDIR Uras 10 E (Hartmann & Braun) for CO and N_2O,

Table 1
Reactant mixture compositions (mol%) for thermal treatments and activity tests

Component	Composition 1	Composition 2	Composition 3
CH_4	0.05	0.05	0.10
CO	0.50	0.50	0.40
NO	–	0.10	–
O_2 (determined by R_x)	0.4200	0.3700 0.3070 0.2965 0.2860	0.4800 0.3840
R_x	1.2	1.2 1.02 0.99 0.96	1.2 0.96
CO_2	10.00	10.00	10.00
H_2O	10.00	10.00	10.00
SO_2	–	0.0008 (optional)	–
N_2	Balance	Balance	Balance

CLD (Grubb Parsons Chemitox) for NO_x and paramagnetic OXYNOS-1 (LEYBOLD-HERAEUS) for O_2, were used for the analysis of the inlet and outlet gas stream.

2.3. Characterization

The powders, thermally treated at 950 °C for 3 h under the mixture with composition no. 3 in Table 1, were characterized by various techniques. X-ray diffraction (XRD) was applied using a Siefert 3003-TT diffractometer, with Fe Kα radiation (λ = 1.9361 Å) in the 2θ range 20–105°, for the identification of the crystal phases. Surface elements atomic concentration and surface ions valence state, were determined by X-ray photoelectron spectroscopy (XPS), using an ultra high vacuum SPECKS LHS-10 system with Al Kα radiation (1486.6 eV). Binding energy measurements of samples that exhibited electrostatic surface charging were corrected with reference to the C 1s peak at 284.4 eV. High resolution transmission electron microscopy (HRTEM), energy dispersive X-ray (EDX) and electron energy loss spectroscopy (EELS) observations were obtained using a Philips CM20 TEM, with ultrathin window energy dispersive X-ray analyzer and Gatan imaging filter (GIF200) for EELS.

3. Results and discussion

3.1. Catalytic activity tests

The CO conversion was between 97 and 99% for $R_x < 1$ and 100% for $R_x > 1$ for all catalysts.

3.1.1. Effect of ageing

Figs. 1a, 1b, 2a and 2b show the 12 h ageing effect for methane oxidation, on $La_{0.91}Mn_{0.85}Ce_{0.24}Pd_{0.05}O_z$, $La_{1.034}Mn_{0.966}Pd_{0.05}O_z$ and the commercial catalyst, under various R_x values (the conversion curves corresponding to 3 and 6 h of ageing are not shown here). The commercial catalyst exhibited high effectiveness in the fresh state. Thermal ageing incurred a severe deactivation to this catalyst for all R_x values. During the first 3 h of ageing, an intense deactivation occurred, followed by further, but less intense, deactivation until the 6th hour of ageing. As shown in Figs. 1 and 2, the catalyst was dramatically deactivated after 12 h. The $La_{0.91}Mn_{0.85}Ce_{0.24}Pd_{0.05}O_z$ catalyst exhibited similar behavior under reducing (R_x = 0.96, Fig. 2b) or around stoichiometric (R_x = 0.99, 1.02, shown in Figs. 2a and 1b, respectively) conditions, but its thermal deactivation was less intense than that of the commercial catalyst. Under oxidizing conditions, R_x = 1.2, $La_{0.91}Mn_{0.85}Ce_{0.24}Pd_{0.05}O_z$ appeared activated after 3 h of ageing, in agreement to previous results obtained with granulated samples in our laboratory [31]. This activation was almost unaffected by up to 6 h of thermal treatment, while a severe deactivation occurred during the last 6 h of ageing (Fig. 1a). A different ageing behavior was observed on $La_{1.034}Mn_{0.966}Pd_{0.05}O_z$. After 3 h of operation at 950 °C, the catalyst exhibited a dramatic activation at R_x = 1.2, which remained unchanged until up to 6 h of ageing. As seen in Fig. 1a, although the last 6 h of ageing induced a deactivation, the 12 h aged $La_{1.034}Mn_{0.966}Pd_{0.05}O_z$ catalyst was more active than the fresh one. This active phase exhibited high thermal stability under around stoichiometric conditions. At R_x = 1.02, the catalyst was activated after the first 3 h, while its performance after 6 and 12 h appeared almost identical to that of the fresh one (Fig. 1b). Under sub-stoichiometric (R_x = 0.99) or reducing (R_x = 0.96) conditions, the catalyst exhibited a mild deactivation, as shown in Fig. 2a and b, respectively.

As can be seen from Figs. 1 and 2, after 12 h of ageing, the Pd/perovskite catalysts exhibited better effectiveness for methane combustion for $R_x > 1$, while the commercial catalyst was superior for $R_x < 1$. The Pd–perovskite catalysts gave high methane conversions (higher than 80%) at temperatures much lower than the commercial one for $R_x < 1$, after ageing.

The 12 h ageing effect for NO reduction on the investigated catalysts at R_x values 1.02, 0.99 and 0.96 is shown in Fig. 3. At R_x = 1.02 (Fig. 3a), the effect of thermal ageing on the performance of the commercial catalyst was more intense. While the commercial catalyst was superior in the fresh state, it exhibited similar effectiveness to that of $La_{1.034}Mn_{0.966}Pd_{0.05}O_z$ after ageing,

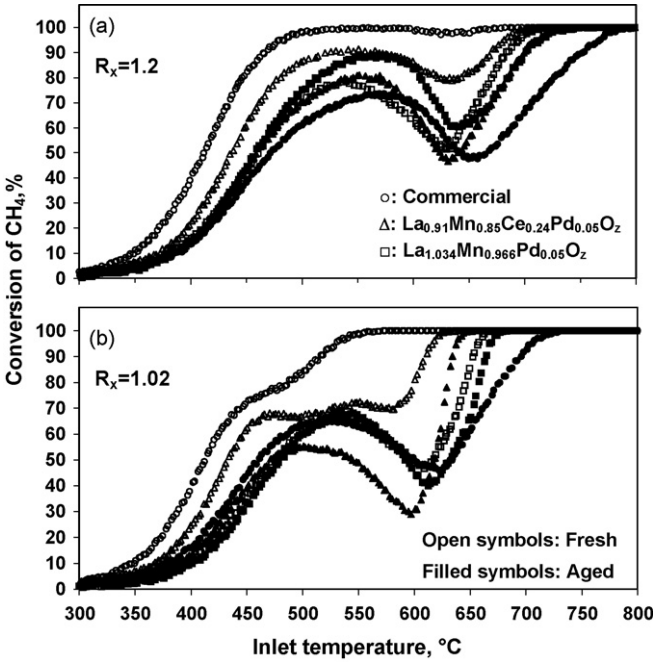

Fig. 1. Temperature dependence of methane conversion of fresh and aged at 950 °C for 12 h catalysts at (a) R_x = 1.2 and (b) R_x = 1.02.

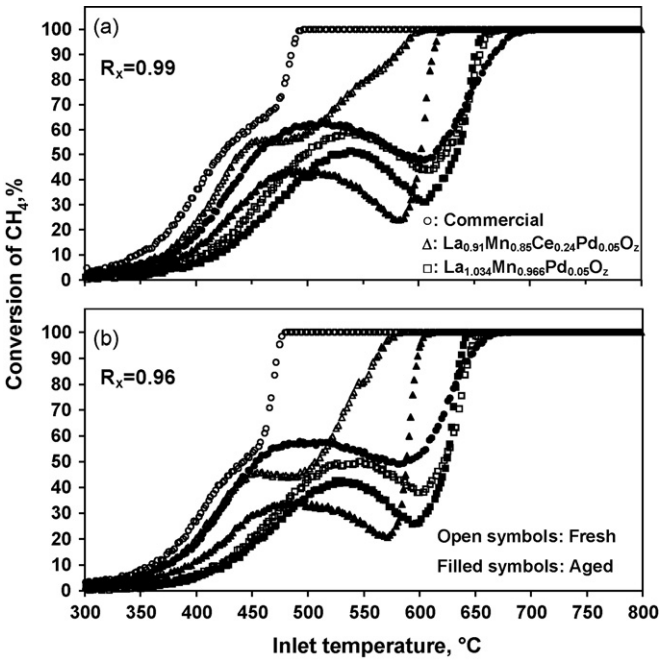

Fig. 2. Temperature dependence of methane conversion of fresh and aged at 950 °C for 12 h catalysts at (a) R_x = 0.99 and (b) R_x = 0.96.

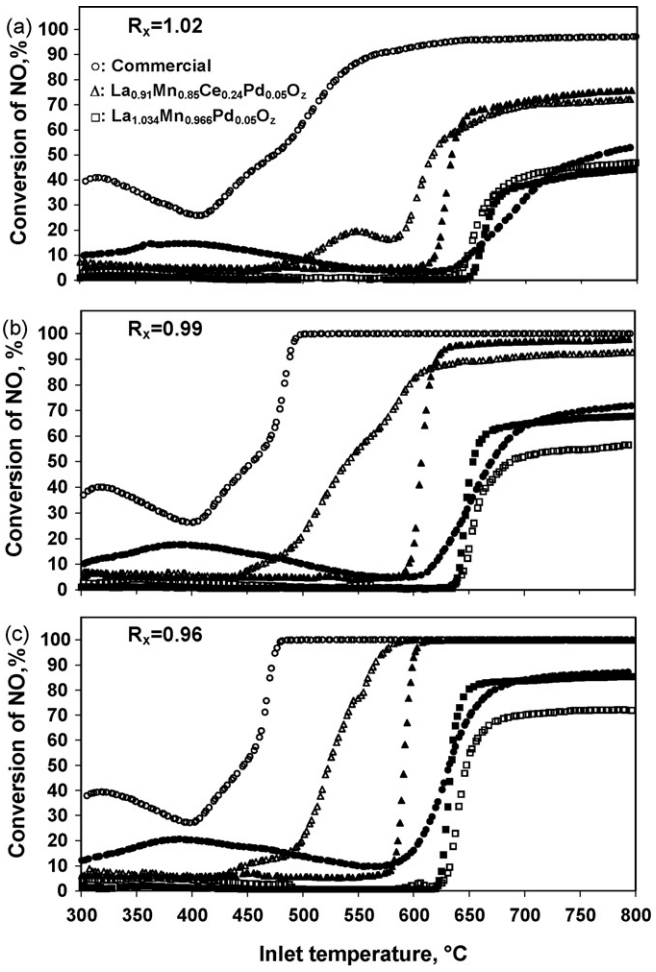

Fig. 3. Temperature dependence of NO conversion at (a) R_x = 1.02, (b) R_x = 0.99 and (c) R_x = 0.96. Open symbols: fresh samples. Filled symbols: aged for 12 h at 950 °C samples.

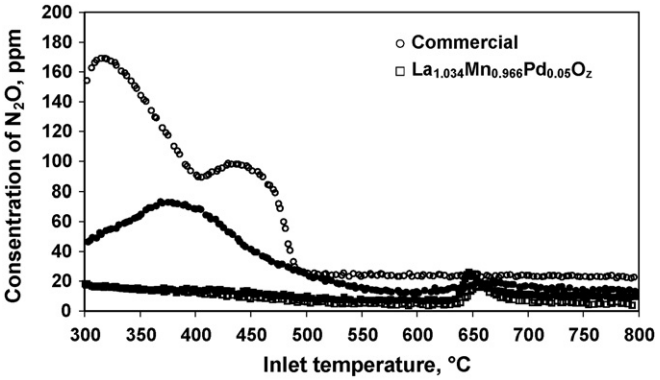

Fig. 4. Temperature dependence of N_2O concentration at R_x = 0.99. Open symbols: fresh samples. Filled symbols: aged for 12 h at 950 °C samples.

despite the fact that the former contained Rh, which exhibits high activity for the reduction of NO. The $La_{0.91}Mn_{0.85}Ce_{0.24}Pd_{0.05}O_z$ catalyst appeared more active for NO_x reduction in all aged states, probably, due to the capability of Ce to act as an oxygen storage component. Similar behavior, but with higher conversions, was observed at R_x values 0.99 and 0.96, as shown in Fig. 3b and c, respectively.

As seen in Fig. 3a–c, the commercial catalyst was more effective in NO conversion at temperatures lower than 550 °C, in both fresh and aged states. Because of the simultaneous N_2O production (Fig. 4), however, the selectivity of the commercial catalyst for the NO reduction to N_2 and O_2, was low. Similar results were obtained at all R_x values.

3.1.2. Effect of SO_2

The continuous operation at temperatures between 300 and 800 °C and under a 8 ppm SO_2 containing reactant mixture, resulted in three different patterns of catalytic behavior, depending on the type of catalyst and on the R_x value. According to the first pattern, a catalytic activation during the first hours of exposure to SO_2 was observed, followed by a continuous deactivation. This behavior was obtained only with the commercial catalyst under highly oxidizing conditions (R_x = 1.2).

In the second pattern, a gradient deactivation from the beginning of the exposure was observed. This was the case of (a) the commercial catalyst operating at R_x = 1.02 and 0.99 (Fig. 5a) and R_x = 0.96 (Fig. 5b), (b) of $La_{0.91}Mn_{0.85}Ce_{0.24}Pd_{0.05}O_z$, under all conditions studied and (c) of $La_{1.034}Mn_{0.966}Pd_{0.05}O_z$, operating under highly oxidizing conditions (R_x = 1.2). The third pattern applies to $La_{1.034}Mn_{0.966}Pd_{0.05}O_z$ only and at R_x = 1.02, 0.99 and 0.96 (Fig. 6a–c, respectively). According to the third pattern, a deactivation occurred during the first few hours of exposure, followed by a gradual activation. The final level of catalytic effectiveness for this catalyst was much higher than the initial one, which was obtained in the absence of SO_2. The aforementioned activation was more noticeable at lower R_x values.

As seen in Fig. 5a, at R_x = 0.99, although the commercial catalyst was more effective in a SO_2-free environment, the $La_{1.034}Mn_{0.966}Pd_{0.05}O_z$ catalyst exhibited higher conversions in the range 470–580 °C after operation for 22 h in a 8 ppm SO_2 containing reactant mixture. At R_x = 0.96, the superiority of the commercial catalyst vs. the $La_{1.034}Mn_{0.966}Pd_{0.05}O_z$, was reduced in the range 350–600 °C (Fig. 5b). This is because of the deactivation of the former and the activation of the latter. Nevertheless, these catalysts exhibited identical performance at temperatures higher than 600 °C. The

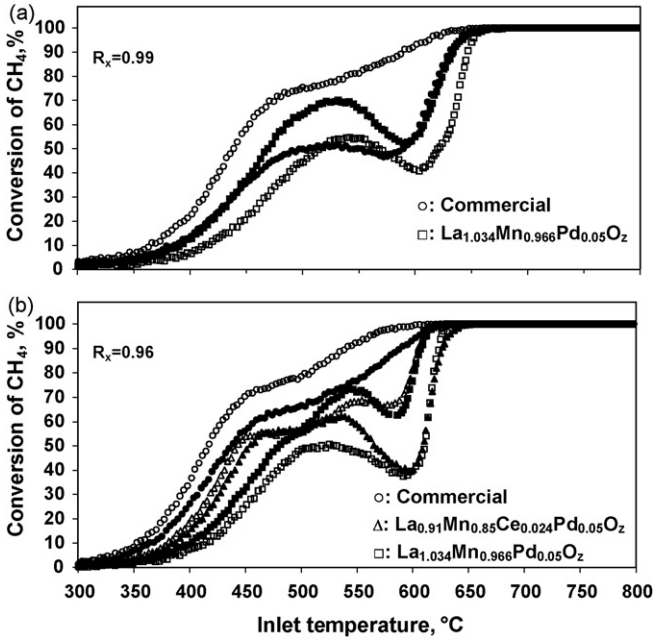

Fig. 5. Effect of SO_2 on the conversion of methane at (a) R_x = 0.99 and (b) R_x = 0.96. Open symbols: no SO_2. Filled symbols: 8 ppm SO_2 for 22 h.

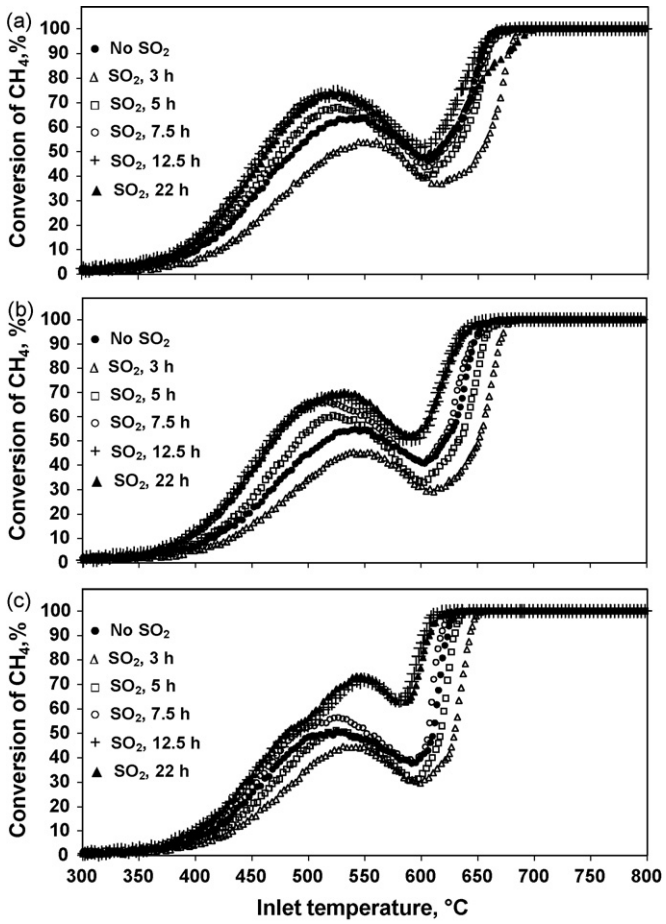

Fig. 6. Effect of SO_2 on the conversion of methane for the $La_{1.034}Mn_{0.966}Pd_{0.05}O_z$ catalyst at (a) $R_x = 1.02$, (b) $R_x = 0.99$ and (c) $R_x = 0.96$.

effect of SO_2 on the effectiveness in NO reduction was more intense for the commercial catalyst, which performed almost identically to $La_{1.034}Mn_{0.966}Pd_{0.05}O_z$ at temperatures higher than 600 °C and at $R_x = 0.99$ (Fig. 7).

3.2. Characterization

The BET specific surface areas (SSA) of the Pd/perovskite active phases were reported earlier [31]. Their values were between 13.6 and 36.8 $m^2\ g^{-1}$, depending on the sample and on the thermal treatment.

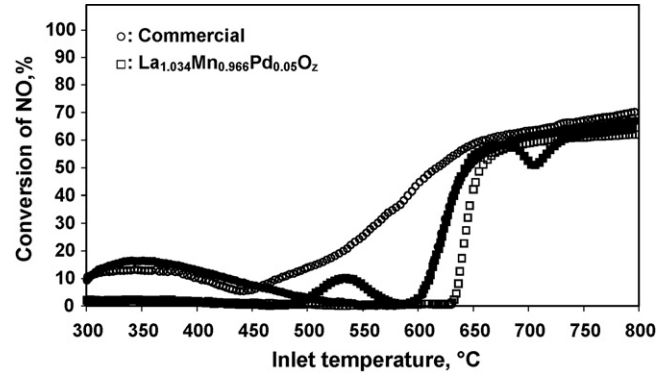

Fig. 7. Effect of SO_2 on the conversion of NO at $R_x = 0.99$. Open symbols: no SO_2. Filled symbols: 8 ppm SO_2 for 22 h.

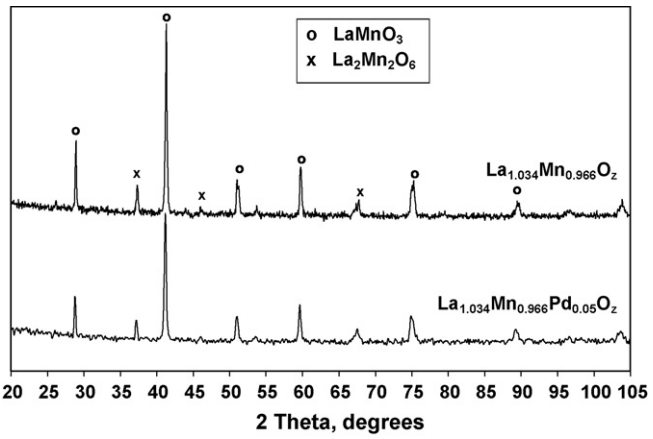

Fig. 8. XRD patterns of the $La_{1.034}Mn_{0.966}Pd_{0.05}O_z$ phase and the pure perovskite substrate $La_{1.034}Mn_{0.966}O_z$, treated at $R_x = 1.2$.

3.2.1. XRD

XRD patterns of the $La_{1.034}Mn_{0.966}Pd_{0.05}O_z$ active phase and of the pure perovskite substrate, $La_{1.034}Mn_{0.966}O_z$, treated under oxidizing conditions ($R_x = 1.2$), are shown in Fig. 8. The double-perovskite structure, $La_2Mn_2O_6$, was detected at a low percentage of 1–3%, together with the main phase of the $LaMnO_3$ perovskite. The XRD results showed that the possibility of Pd insertion in the double-perovskite structure was very high. As reported previously [31], the migration of Pd out of the perovskite lattice is the most probable cause of the activation of $La_{0.91}Mn_{0.85}Ce_{0.24}Pd_xO_z$, with $x = 0.1$, after thermal ageing under oxidative reaction conditions. In this work, no segregated Pd was detected in the XRD patterns of $La_{1.034}Mn_{0.966}Pd_{0.05}O_z$. Neither segregated La was observed, despite its excess in the perovskite nominal formulation. These observations imply the formation of mixed La–Pd oxides. It was found [32] that insertion of Pd^{x+} ($x > 2$), in the perovskite structure, does not ensure the conservation of its oxidized form, while segregated PdO on the surface can be easily reduced. Thus, it is suggested that Pd could be protected against reduction either by its insertion to the $La_2Mn_2O_6$ structure, or by forming mixed oxides with La, thus resulting in highly active catalysts for methane combustion.

Fig. 9a and b shows the XRD spectra of $La_{0.91}Mn_{0.85}Ce_{0.24}Pd_{0.05}O_z$ and $La_{1.034}Mn_{0.966}Pd_{0.05}O_z$, respectively, after treatment under oxidizing ($R_x = 1.2$) and reducing ($R_x = 0.96$) conditions. Fig. 9a shows that for the $La_{0.91}Mn_{0.85}Ce_{0.24}Pd_{0.05}O_z$, the peaks of the double perovskite at $R_x = 1.2$ were almost absent, while at $R_x = 0.96$, a peak at 37.3° was obtained. The peaks of the $La_2Mn_2O_6$ phase were detected in the patterns of $La_{1.034}Mn_{0.966}Pd_{0.05}O_z$ for both R_x values, but were less intense under reducing conditions. The lower crystallization extent of the double perovskite could imply that part of the excess La, formed a more active mixed La–Pd oxide, thus providing thermal stability under reducing conditions, as shown in Fig. 2a and b.

Fig. 10 shows that the only detectable structural change that occurred to $La_{1.034}Mn_{0.966}Pd_{0.05}O_z$ after treatment with 8 ppm SO_2, was a shift of the peaks to lower 2θ values.

3.2.2. XPS

Table 2 summarizes the surface composition data of $La_{0.91}Mn_{0.85}Ce_{0.24}Pd_{0.05}O_z$ and $La_{1.034}Mn_{0.966}Pd_{0.05}O_z$ after various treatments. It can be seen that thermal treatment at $R_x = 1.2$, induced enrichment in the surface La of $La_{1.034}Mn_{0.966}Pd_{0.05}O_z$. Further and more extended enrichment in the surface La occurred after thermal treatment of this sample under reducing conditions.

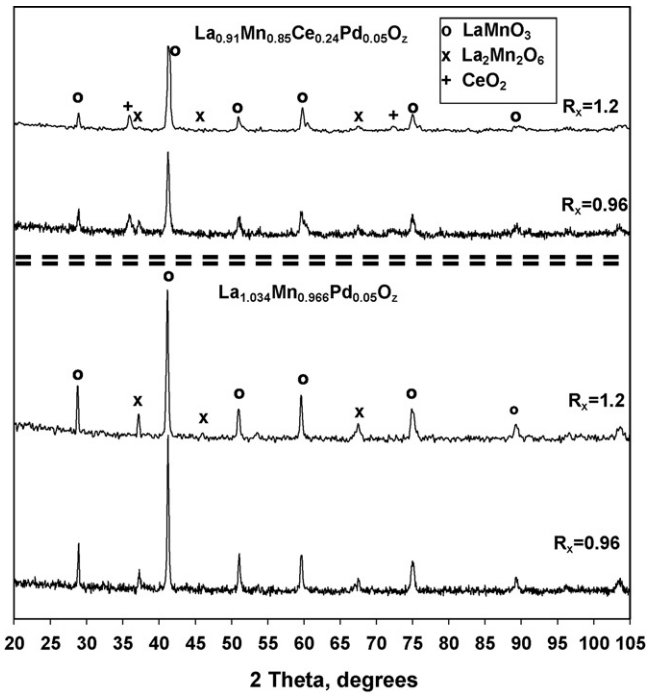

Fig. 9. XRD patterns of the (a) $La_{0.91}Mn_{0.85}Ce_{0.24}Pd_{0.05}O_z$ and (b) $La_{1.034}Mn_{0.966}Pd_{0.05}O_z$ active phases treated at $R_x = 1.2$ and 0.96.

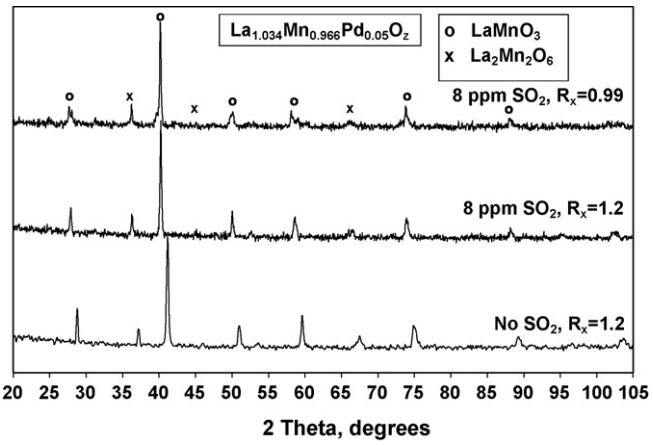

Fig. 10. XRD patterns of the $La_{1.034}Mn_{0.966}Pd_{0.05}O_z$ active phase treated at $R_x = 1.2$ and 0.99 under reactant mixture with 8 ppm SO_2.

The same was observed for surface Pd. On the contrary, the surface Mn appeared decreased. A similar behavior for La and Mn, was observed with $La_{0.91}Mn_{0.85}Ce_{0.24}Pd_{0.05}O_z$, in which, however, the surface Pd was decreased. The enhanced La and Pd surface compositions of the reduced $La_{1.034}Mn_{0.966}Pd_{0.05}O_z$ catalyst could increase the possibilities of formation of mixed La–Pd oxides, which probably, increased thermal stability. Compared to the oxidized sample, the SO_2-treated $La_{1.034}Mn_{0.966}Pd_{0.05}O_z$ exhibited slight surface La increase and Mn decrease. The surface was enriched in Pd in both samples, especially for that with $R_x = 0.99$, while the surface composition in sulfur on the total surface elements basis was 1.64 and 0.93% for $R_x = 1.2$ and 0.99, respectively.

The binding energies (BEs) of the elements are shown in Table 3. As reported previously [31], the BEs of La3d and Mn2p provided strong evidence for the formation of the $LaMnO_3$ perovskite on the catalytic surface. The BEs of Ce3d at 881.9 ± 0.3 eV have been ascribed to Ce^{4+} [33], which, probably corresponds to segregated CeO_2. An XPS peak fitting commercial software (XPSPeak Version 4.1) was used for the Pd3d peaks analysis. The total Pd3d peak, in some cases, consisted of two peaks. The first appeared at approximately 337.0 eV and corresponded to oxidized Pd^{2+} [33]. The second appeared at BEs around 339.0 eV and referred to oxidized Pd^{x+}, $x > 2$ [33]. Such BEs were ascribed to cationic Pd^{3+} or Pd^{4+}, inserted at the B-site of the $LaFe_{0.95}Pd_{0.05}O_3$ perovskite under oxidizing conditions [34]. Table 4 lists the BEs and the % proportion of the Pd3d peaks that resulted by peak analysis. It can be seen that in either the fresh or in the treated under oxidizing conditions $La_{1.034}Mn_{0.966}Pd_{0.05}O_z$ sample, about 16.7% of the surface Pd, which was in the form Pd^{3+} or Pd^{4+}, was inserted in the perovskite structure [34,35]. Thermal treatment under reducing conditions increased the Pd insertion to 20%. These observations can explain the unchanged effectiveness after ageing at $R_x = 1.02$ (Fig. 2) and the mild deactivation after ageing at $R_x = 0.99$ and 0.96 (Fig. 3). Treatment of this catalyst with SO_2, resulted in complete migration of Pd out of the perovskite lattice with a simultaneous increase in the surface Pd content, providing evidence for the enhanced activity under SO_2 environment. The Pd3d peak at 334.6 eV of the reduced $La_{0.91}Mn_{0.85}Ce_{0.24}Pd_{0.05}O_z$ sample, can be ascribed to metallic Pd [33]. The decreased surface Pd composition

Table 2
XPS surface and nominal bulk composition of fresh, thermally and SO_2-treated catalysts

Catalyst	La (mol%)		Mn (mol%)		Ce (mol%)		Pd (mol%)	
	Surface	Bulk	Surface	Bulk	Surface	Bulk	Surface	Bulk
Fresh catalysts								
$La_{0.91}Mn_{0.85}Ce_{0.24}Pd_{0.05}O_z$	38.4	44.4	44.3	41.5	15.4	11.7	1.9	2.4
$La_{1.034}Mn_{0.966}Pd_{0.05}O_z$	46.0	50.4	52.1	47.1	–	–	1.9	2.4
[a]Aged under oxidizing conditions								
$La_{0.91}Mn_{0.85}Ce_{0.24}Pd_{0.05}O_z$	39.0	44.4	42.3	41.5	17.1	11.7	1.7	2.4
$La_{1.034}Mn_{0.966}Pd_{0.05}O_z$	49.0	50.4	49.6	47.1	–	–	1.4	2.4
[b]Aged under reducing conditions								
$La_{0.91}Mn_{0.85}Ce_{0.24}Pd_{0.05}O_z$	43.1	44.4	41.9	41.5	13.8	11.7	1.2	2.4
$La_{1.034}Mn_{0.966}Pd_{0.05}O_z$	55.2	50.4	43.1	47.1	–	–	1.8	2.4
[c]Aged SO_2-treated catalysts								
$La_{1.034}Mn_{0.966}Pd_{0.05}O_z$, $R_x = 1.2$	50.2	50.4	48.0	47.1	–	–	1.8	2.4
$La_{1.034}Mn_{0.966}Pd_{0.05}O_z$, $R_x = 0.99$	51.7	50.4	46.1	47.1	–	–	2.2	2.4

[a] Thermally treated, 950 °C for 3 h under composition 3 with $R_x = 1.2$.
[b] Thermally treated, 950 °C for 3 h under composition 3 with $R_x = 1.2$ and thermally treated from 950 to 300 °C for 1 h under composition 3 with $R_x = 0.96$.
[c] Thermally treated, 950 °C for 3 h under composition 1 and SO_2-treated in the range 300–450 °C for 7.5 h under composition 2 with $R_x = 1.2$ and 0.99.

Table 3
Binding energies (eV) of elements in fresh, thermally and SO_2-treated samples

Catalyst	La	Mn	Ce	Pd	S
Fresh catalysts					
$La_{0.91}Mn_{0.85}Ce_{0.24}Pd_{0.05}O_z$	834.2	641.8	881.9	337.3	–
$La_{1.034}Mn_{0.966}Pd_{0.05}O_z$	833.8	641.9	–	336.9	–
[a]Aged under oxidizing conditions					
$La_{0.91}Mn_{0.85}Ce_{0.24}Pd_{0.05}O_z$	834.5	641.8	882.0	337.1	–
$La_{1.034}Mn_{0.966}Pd_{0.05}O_z$	834.1	641.6	–	336.9	–
[b]Aged under reducing conditions					
$La_{0.91}Mn_{0.85}Ce_{0.24}Pd_{0.05}O_z$	834.3	641.6	882.0	336.7	–
$La_{1.034}Mn_{0.966}Pd_{0.05}O_z$	834.5	641.7	–	336.8	–
[c]Aged SO_2-treated catalysts					
$La_{1.034}Mn_{0.966}Pd_{0.05}O_z$, $R_x = 1.2$	834.2	641.7	–	336.9	168.5
$La_{1.034}Mn_{0.966}Pd_{0.05}O_z$, $R_x = 0.99$	834.7	641.7	–	337.1	168.5

[a] Thermally treated, 950 °C for 3 h under composition 3 with $R_x = 1.2$.
[b] Thermally treated, 950 °C for 3 h under composition 3 with $R_x = 1.2$ and thermally treated from 950 to 300 °C for 1 h under composition 3 with $R_x = 0.96$.
[c] Thermally treated, 950 °C for 3 h under composition 1 and SO_2-treated in the range 300–450 °C for 7.5 h under composition 2 with $R_x = 1.2$ and $R_x = 0.99$.

Table 4
BEs and % proportion of Pd 3d peaks that resulted by total peak analysis

Catalyst	BE peak 1 (eV)	BE peak 2 (eV)	% peak1–% peak2
	Pd^{2+}	Pd^{x+}, $x > 2$	
Fresh catalysts			
$La_{0.91}Mn_{0.85}Ce_{0.24}Pd_{0.05}O_z$	337.3	–	100.0–0.0
$La_{1.034}Mn_{0.966}Pd_{0.05}O_z$	336.9	339.2	83.3–16.7
[a]Aged under oxidizing conditions			
$La_{0.91}Mn_{0.85}Ce_{0.24}Pd_{0.05}O_z$	336.9	338.9	76.9–23.1
$La_{1.034}Mn_{0.966}Pd_{0.05}O_z$	336.9	339.2	83.3–16.7
[b]Aged under reducing conditions			
$La_{0.91}Mn_{0.85}Ce_{0.24}Pd_{0.025}O_z$	336.8	334.6[d]	74.1–25.9[d]
$La_{1.034}Mn_{0.966}Pd_{0.05}O_z$	336.7	339.0	80.0–20.0
[c]Aged SO_2-treated catalysts			
$La_{1.034}Mn_{0.966}Pd_{0.05}O_z$, $R_x = 1.2$	337.0	–	100.0–0.0
$La_{1.034}Mn_{0.966}Pd_{0.05}O_z$, $R_x = 0.99$	337.0	–	100.0–0.0

[a] Thermally treated, 950 °C for 3 h under composition 3 with $R_x = 1.2$.
[b] Thermally treated, 950 °C for 3 h under composition 3 with $R_x = 1.2$ and thermally treated from 950 to 300 °C for 1 h under composition 3 with $R_x = 0.96$.
[c] Thermally treated, 950 °C for 3 h under composition 1 and SO_2-treated in the range 300–450 °C for 7.5 h under composition 2 with $R_x = 1.2$ and 0.99.
[d] Corresponds to metallic Pd.

and the partial reduction of oxidized Pd to metallic Pd are the reasons for the deactivation of this catalyst under reducing conditions (Fig. 2). The latter was not observed with $La_{1.034}Mn_{0.966}Pd_{0.05}O_z$, in which Pd appeared to be protected from reduction. The sulfur peaks

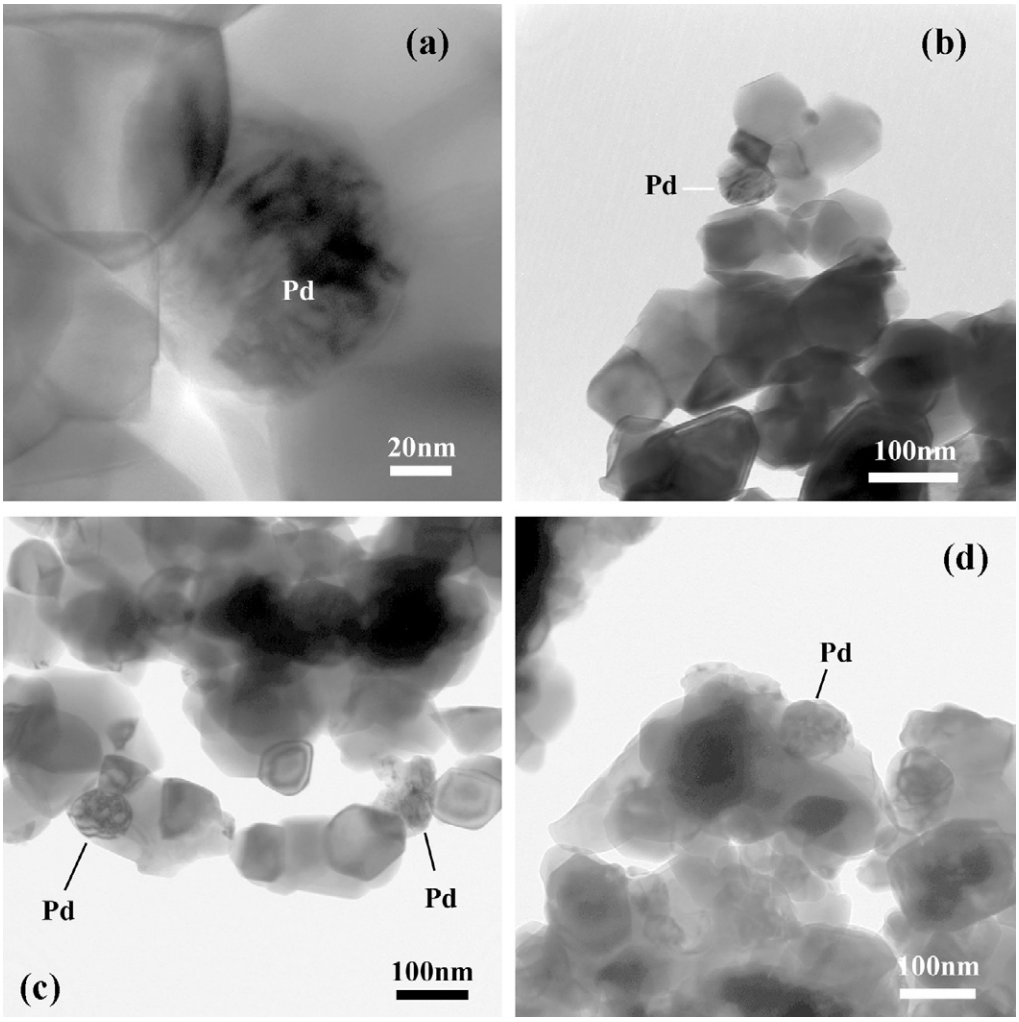

Fig. 11. HRTEM micrographs of the $La_{1.034}Mn_{0.966}Pd_{0.05}O_z$ catalyst. (a) and (b) fresh; (c) and (d) aged for 3 h at 950 °C ($R_x = 1.2$).

of the SO_2-treated samples were detected at 168.5 eV and can be attributed to surface sulfates [33]. The higher surface sulfur content in the treated at R_x = 1.2 sample (1.64% vs. 0.93% at R_x = 0.99), could possibly mean that sulfur attack affects more intensely the catalytic effectiveness under oxidizing conditions, which is in agreement with the results of the activity tests.

3.2.3. EDX, HRTEM and EELS

EDX measurements were conducted on the $La_{1.034}Mn_{0.966}Pd_{0.05}O_z$, $La_{1.034}Mn_{0.966}O_z$, and $La_{0.966}Mn_{1.034}Pd_{0.05}O_z$ samples. In the latter, which was found to be inactive in methane combustion, about 33% of its surface Pd was in the metallic form [31]. The average (%) stoichiometry of La/Mn on each particle of the above samples was 60/40, 58/42 and 55/45, respectively.

HRTEM and EELS were carried out on fresh and thermally treated (for 3 h at 950 °C, R_x = 1.2) $La_{1.034}Mn_{0.966}Pd_{0.05}O_z$. As seen in Fig. 11a and b for the fresh sample, the size of Pd crystallites was approximately 50 nm, while the $LaMnO_3$ crystallites were between 50 and 100 nm. Thermal treatment incurred an increase of the perovskite crystallites size (mostly higher than 100 nm as seen in Fig. 11c and d), but did not affect considerably the Pd crystallites. The size of $LaMnO_3$ crystallites was also calculated using the Scherrer equation. The values were about 55 and 75 nm for the fresh and for the thermally treated samples, respectively. There is a large difference between the crystallite sizes obtained by the two methods, probably because the $LaMnO_3$ particles examined by HRTEM consisted of aggregates of many particles. However, the increase of the crystallite size in both cases shows a slight sintering, which is confirmed by the lower BET surface area after ageing [31]. No Pd was detected in the perovskite crystallites. The bulk oxygen content of the Pd crystallites corresponded to PdO_x with x close to 0, meaning that bulk Pd was almost metallic (Fig. 12). Taking into account the XPS results, which showed that surface Pd was oxidized, it can be considered that the Pd particles consisted of a metallic core, covered with a catalytically active oxide layer. This is in agreement with Cimino et al. [35], who found that the active form for the oxidation of methane on a Pd–$LaMnO_3$ catalyst was PdO over metallic Pd. Cimino et al. observed catalyst activation after thermal treatment at temperatures higher than those corresponding to PdO_x decomposition. This activation was ascribed to the formation of metallic Pd on the catalytic surface (confirmed by XPS), with simultaneous decrease of high valenced Pd. The very active PdO–Pd sites were metastable and were reoxidized after operation at lower temperatures, thus causing a deactivation with time.

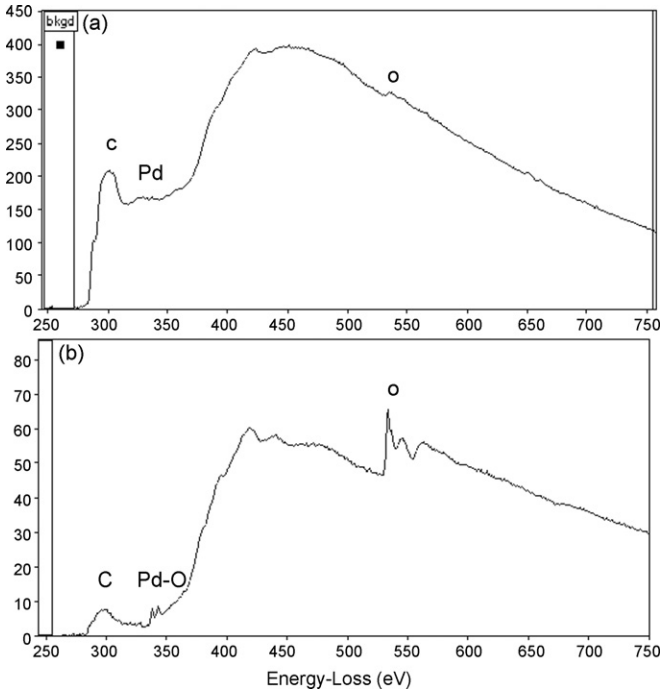

Fig. 12. EELS spectra of (a) a Pd particle in the $La_{1.034}Mn_{0.966}Pd_{0.05}O_z$ aged for 3 h at 950 °C (R_x = 1.2) catalyst and (b) reference spectrum of PdO for comparison.

In this study, no metallic Pd was detected on the $La_{1.034}Mn_{0.966}Pd_{0.05}O_z$ surface. Moreover, HRTEM and EELS results provided strong evidence for the coexistence of La (and to less extent Mn) in the Pd crystallites, especially in the thermally treated sample. Thus, it is suggested that part of the excess La in the catalyst formula was inserted into the surface oxide layer of the Pd crystallites, forming mixed La–Pd oxides. These oxides, probably, induce stability against complete oxidation or reduction of Pd, which can cause deactivation. Further stability appears to be provided by the increased Pd crystallite size, which retards the rate of reoxidation of the active PdO–Pd sites [35]. Similarly, part of the surface Mn could have formed a La–Mn double perovskite, in which Mn was substituted by Pd.

The high surface composition in Pd^{2+} (2.2%), the surface enrichment in La and the low surface composition in sulfur (0.93%) of the sample treated in SO_2 at R_x = 0.99, combined with the HRTEM and EELS results, could explain the positive effect of SO_2 on the catalytic activity of $La_{1.034}Mn_{0.966}Pd_{0.05}O_z$.

4. Conclusions

Thermal ageing affects strongly the catalytic effectiveness of $La_{0.91}Mn_{0.85}Ce_{0.24}Pd_{0.05}O_z$, $La_{1.034}Mn_{0.966}Pd_{0.05}O_z$ and commercial Pd-based three-way catalysts for stoichiometrically operating NGFVs. The Pd/perovskites, especially $La_{1.034}Mn_{0.966}Pd_{0.05}O_z$, exhibit higher thermal stability than the commercial catalyst. This enhanced stability can be attributed to the formation either of mixed La–Pd oxides and/or of a La–Mn double perovskite.

Introduction of 8 ppm SO_2 in the reactant mixture induces a severe deactivation on $La_{0.91}Mn_{0.85}Ce_{0.24}Pd_{0.05}O_z$ and on the commercial catalyst. The $La_{1.034}Mn_{0.966}Pd_{0.05}O_z$ catalyst appears activated under reducing or close to stoichiometric conditions. This activation can be ascribed to the enhanced surface Pd^{2+} and La compositions, which favor the formation of mixed La–Pd oxides, and to the low surface sulfur composition.

The thermal ageing durability and the activation of $La_{1.034}Mn_{0.966}Pd_{0.05}O_z$ in the presence of SO_2, imply that this catalyst can be a potential substitute of the currently used commercial catalysts that contain almost threefold higher noble metal loads.

Acknowledgement

The authors gratefully acknowledge the European Union for the funding (project CAT-NAT: Cost-Effective and Durable Nanostructured Pd Catalysts for Natural gas Vehicle and premixed Burner Applications) under contract G5RD-CT2001-00567.

References

[1] T. Seiyama, in: L.G. Tejuka, J.L.G. Fierro (Eds.), Properties and Applications of Perovskite-type Oxides, Marcel Dekker, 1993, p. 215.
[2] H. Arai, T. Yamada, K. Eguchi, T. Seiyama, Appl. Catal. 26 (1986) 265.
[3] M. Hackenberger, K. Stephan, D. Kieβling, W. Schmitz, G. Wendt, Solid State Ionics 101–103 (1997) 1195.
[4] R. Leanza, I. Rossetti, L. Fabbrini, C. Oliva, L. Forni, Appl. Catal. B: Environ. 28 (2000) 55.
[5] A.E. Giannakas, A.K. Ladavos, P.J. Pomonis, Appl. Catal. B: Environ. 49 (2004) 147.

[6] A.E. Giannakas, A.A. Leontiou, A.K. Ladavos, P.J. Pomonis, Appl. Catal. A: Gen. 309 (2006) 254.
[7] G. Pecchi, P. Reyes, R. Zamora, C. Campos, L.E. Cadus, B.P. Barbero, Catal. Today 133–135 (2008) 420.
[8] F.H. Ribeiro, M. Chow, R.A. Dalla Betta, J. Catal. 146 (1994) 537.
[9] R. Burch, F.J. Urbano, P.K. Loader, Appl. Catal. A: Gen. 123 (1995) 173.
[10] R. Burch, Catal. Today 35 (1997) 27.
[11] P. Gelin, L. Urfels, M. Primet, E. Tena, Catal. Today 83 (2003) 45.
[12] R. Zhang, H. Alamdari, S. Kaliaguine, Appl. Catal. B: Environ. 72 (2007) 331.
[13] J.K. Lampert, M. Shahjahan Kazi, R.J. Farrauto, Appl. Catal. B: Environ. 14 (1997) 211.
[14] D.D. Beck, J.W. Sommers, Appl. Catal. B: Environ. 6 (1995) 185.
[15] L.F. Liotta, G. Di Carlo, G. Pantaleo, A.M. Venezia, G. Deganello, E. Merlone Borla, M. Pidria, Appl. Catal. B: Environ. 75 (2007) 182.
[16] D.L. Mowery, M.S. Graboski, T.R. Ohno, R.L. McCormick, Appl. Catal. B: Environ. 21 (1999) 157.
[17] V. Meeyoo, D.L. Trimm, N.W. Cant, Appl. Catal. B: Environ. 16 (1998) L101.
[18] K. Wilson, C. Hardacre, R.M. Lambert, J. Phys. Chem. 99 (1995) 13755.
[19] R. Burch, E. Halpin, M. Hayes, K. Ruth, J.A. Sullivan, Appl. Catal. B: Environ. 19 (1998) 199.
[20] R. Burch, D.J. Crittle, B.W.L. Southward, J.A. Sullivan, Catal. Lett. 72 (2001) 153.
[21] L. Wan, in: L.G. Tejuka, J.L.G. Fierro (Eds.), Properties and Applications of Perovskite-type Oxides, Marcel Dekker, 1993, p. 145.
[22] I. Rosso, E. Garrone, F. Geobaldo, B. Onida, G. Saracco, V. Specchia, Appl. Catal. B: Environ. 30 (2001) 61.
[23] I. Rosso, E. Garrone, F. Geobaldo, B. Onida, G. Saracco, V. Specchia, Appl. Catal. B: Environ. 34 (2001) 29.
[24] I. Rosso, G. Saracco, V. Specchia, E. Garrone, Appl. Catal. B: Environ. 40 (2003) 195.
[25] Y. Zhang-Steenwinkel, H.L. Castricum, J. Beckers, E. Eiser, A. Bliek, J. Catal. 221 (2004) 523.
[26] M. Alifanti, R. Auer, J. Kirchnerova, F. Thyrion, P. Grange, B. Delmon, Appl. Catal. B: Environ. 41 (2003) 71.
[27] Y. Zhu, R. Tan, J. Feng, S. Ji, L. Cao, Appl. Catal. A: Gen. 209 (2001) 71.
[28] A. Civera, G. Negro, S. Specchia, G. Saracco, V. Specchia, Catal. Today 100 (2005) 275.
[29] B. Kucharczyk, W. Tylus, Catal. Today 90 (2004) 121.
[30] M.J. Koponen, T. Venalainen, M. Suvanto, K. Kallinen, T.-J.J. Kinnunen, M. Harkonen, T.A. Pakanen, J. Mol. Catal. A: Chem. 258 (2006) 246.
[31] E. Tzimpilis, N. Moschoudis, M. Stoukides, P. Bekiaroglou, Preparation, active phase composition and Pd content of perovskite-type oxides, Appl. Catal. B: Environ. 84 (2008) 607.
[32] H. Tanaka, I. Tan, M. Uenishi, M. Taniguchi, M. Kimura, Y. Nishihata, J. Mizuki, J. Alloys Compd. 408–412 (2006) 1071.
[33] NIST X-ray Photoelectron Spectroscopy Standard Reference Database 20, Version 3.2, National Institute of Standards and Technology, USA, 2000.
[34] M. Uenishi, M. Taniguchi, H. Tanaka, M. Kimura, Y. Nishihata, J. Mizuki, T. Kobayashi, Appl. Catal. B: Environ. 57 (2005) 267.
[35] S. Cimino, M.P. Casaletto, L. Lisi, G. Russo, Appl. Catal. A: Gen. 327 (2007) 238.